ELSEVIER

Thermochimica Acta 391 (2002) 185–196

thermochimica acta

www.elsevier.com/locate/tca

Specific heat capacities and thermal properties of a homogeneous ethylene-1-butene copolymer by adiabatic calorimetry

P.J. van Ekeren[a,*], L.D. Ionescu[a], V.B.F. Mathot[b], J.C. van Miltenburg[a]

[a]*Chemical Thermodynamics Group, Debye Institute, Utrecht University, Padualaan 8, 3584 CH Utrecht, The Netherlands*
[b]*DSM Research, P.O. Box 18, 6160 MD Geleen, The Netherlands*

Received 21 September 2001; accepted 23 October 2001

Abstract

Specific heat capacities of a homogeneous ethylene-1-butene copolymer were measured by adiabatic calorimetry in the temperature range from 7 to 406 K (stepwise heating after cooling at rates in the range from 6 to 25 K h^{-1}, averaged heating rates 5–34 K h^{-1}). The glass transition is centred around 224 K. With devitrification also melting sets in. The crystallinity of the polymer was calculated (within the two-phase model) as a function of temperature using two sets of reference data (one for linear and branched polyethylenes (BPEs), and the other for strictly linear polyethylene (LPE)) for completely crystalline and for completely amorphous material. On heating, the mass fraction crystallinity decreased from 0.30 to 0 in the temperature range from 220 to 360 K, confirming earlier differential scanning calorimetry (DSC) heat capacity measurements. During the stabilisation periods in the melting region negative temperature drifts, related to endothermic effects caused by melting, were observed below 325 K. However, in the temperature range from 325 K up to the end melting temperature, 360 K, positive drifts were measured, reflecting exothermic effects which are attributed to recrystallisation phenomena.

Keywords: Adiabatic calorimetry; Crystallinity; Ethylene-1-butene copolymer; Heat capacity; Polyethylene; Recrystallisation; Relaxation

1. Introduction

To support studies on the thermal behaviour of polymers, which are usually performed using differential scanning calorimetry (DSC) [1], it was decided to measure the heat capacity of some ethylene-1-alkene copolymers very accurately over a wide temperature range using adiabatic calorimetry. The results for a heterogeneous ethylene-1-octene very low density polyethylene (VLDPE) with a comonomer content of 6.2 mol% and a density of 902 kg m^{-3} and for a homogeneous ethylene-1-octene copolymer with a comonomer content of 13.6 mol% and a density of 870 kg m^{-3} have been published previously [2,3]. In this paper, data are presented for a homogeneous ethylene-1-butene copolymer with a comonomer content of 12.9 mol% and a density of 878 kg m^{-3}. With this contribution we would like to express our appreciation to Dr. M. Richardson and to Dr. G. Höhne for their pioneering research in developing techniques and methods for calorimetry and for their commitment to perform quantitative calorimetry for better understanding of the thermal behaviour of polymers.

* Corresponding author. Tel.: +31-30-2533509; fax: +31-30-2533947.
E-mail address: ekeren@chem.uu.nl (P.J. van Ekeren).

0040-6031/02/$ – see front matter
PII: S0040-6031(02)00176-4

2. Experimental

2.1. The sample

The sample, EB 5, is a homogeneous ethylene-1-butene copolymer [4,5] which was produced using metallocene based catalysis. The molar percentage of 1-butene is 12.9% (i.e. the mass percentage of 1-butene is 22.9% by NMR). Its meltindex, I_2, is 9.76 dg/min and the density of the material (at 298 K, after compression moulding) is 878 kg m^{-3}.

2.2. The adiabatic calorimeter

The measurements were performed using one of our home-built adiabatic calorimeters [6,7]. The temperature is measured using a 27 Ω rhodium–iron resistance, which has been calibrated by Oxford Instruments at 33 points between 1.5 and 300 K. The calibration was extended to 430 K using the melting temperatures of naphthalene and indium. Conversion to the ITS-90 scale [8] is based on the article of Goldberg and Weir [9].

After filling and successive evacuation of the calorimeter vessel, helium gas is admitted to the vessel until the pressure is about 1000 Pa. Measurements are made in the intermittent mode. This implies that stabilisation periods are followed by input periods under automatic control. During the stabilisation periods, the temperature is recorded as a function of time. Between two stabilisation periods, an input period is used to raise the temperature of the sample (and vessel). The amount of heat added to the calorimeter vessel is measured very accurately. The temperature increase, which is caused by the heat input, follows from extrapolation of the temperature–time curves of both stabilisation periods. These data allow for the accurate calculation of the heat capacity. The heat capacity of the sample is obtained by subtracting the heat capacity of the empty calorimeter vessel. In the transition regions thermal equilibrium is not reached within a practical time limit because of various kinds of temperature–time dependent processes. Therefore, in these regions another method was applied. The known heat transfer to the surroundings (from an empty vessel experiment) and the amount of heat added to the calorimeter vessel were used to calculate the enthalpy increment between (the midpoints of) two successive stabilisation periods. This results in the actual enthalpy path of the vessel and its content.

Due to the adiabatic construction the heat exchange with the surroundings is very small. Therefore, temperature drifts observed in the stabilisation periods may be used to investigate the temperature–time dependent processes. According to measurements of standard materials, the inaccuracy is approximately 0.2% of the absolute heat capacity.

2.3. The measurements

The calorimeter vessel was filled with an amount of 5.52958 g of the polymer. Eight series of measurements were performed with this sample in the temperature range from 7 to 406 K. An overview of the performed measurements (temperature ranges, duration of stabilisation and input periods and averaged heating rates) is given in Table 1. The sample was cooled after series 1 and 3 by switching off the temperature control of the shields. This resulted in

Table 1
Overview of the series of measurements performed on the EB 5 sample

Series no.	T_1 (K)	T_2 (K)	t (stabilisation) (s)	t (input) (s)	$\langle\beta\rangle$ (K h^{-1})
1	298	389	600	708	5
2	85	113	600	708	7
3	116	385	600	708	6
4	7	31	100	100	34
5	7	29	200	100	20
6	9	100	600	608	8
7	98	279	800	808	5
8	280	406	800	808	4

For each measurement series the temperature range in which measurements were performed is given together with the duration of the stabilisation and input periods and the averaged heating rates $\langle\beta\rangle$.

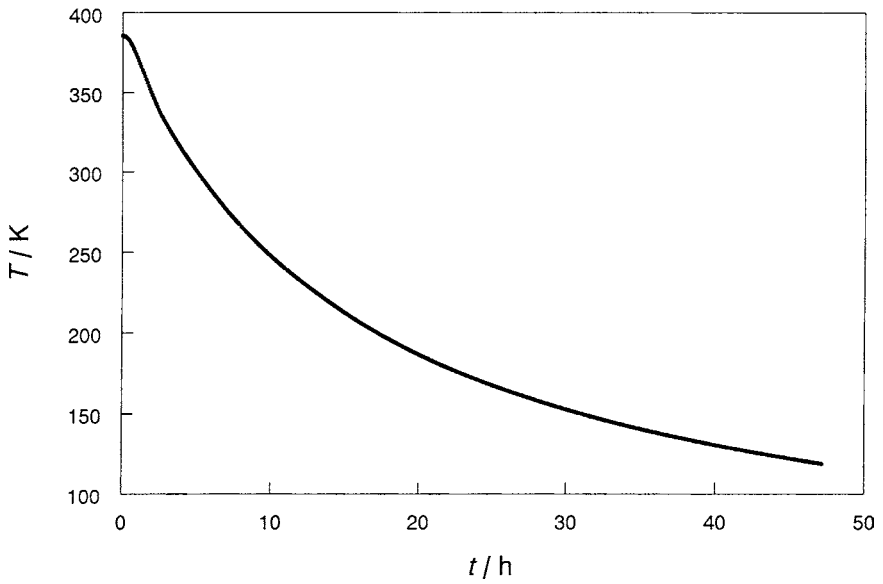

Fig. 1. Cooling curve, recorded after measurement series 3.

a (slow) exponential decrease of the temperature: at 360 K the cooling rate was approximately 25 K h^{-1} and at 220 K the cooling rate was approximately 6 K h^{-1}. To have an impression of the thermal history of the sample the cooling curve which was recorded after series 3 is plotted in Fig. 1.

3. Results and discussion

3.1. Specific heat capacity

The specific heat capacities that were evaluated from the measurements are given in Table 2 and graphically presented in Fig. 2. For temperatures below 315 K the heat capacities measured in series 1 are considerably lower than those measured in series 3 and 8 at the same temperatures. In the temperature range from 315 to 370 K, on the other hand, the heat capacities measured during series 1 are significantly higher than those measured during series 3 and 8. This is caused by the different thermal history of the sample for these measurements. Series 1 was performed on the polymer as received, i.e. on material that had been stored for a long time (years) at room temperature. During the storage the material had obviously relaxed to a more stable state. The first measurements of series

Table 2
Measured specific heat capacity of EB 5 as a function of temperature

T/K	$\frac{C_p}{J K^{-1} g^{-1}}$
Series 1	
298.02	2.384
298.96	2.417
300.41	2.442
302.35	2.480
304.29	2.519
306.20	2.562
308.09	2.613
309.95	2.674
311.76	2.756
313.48	2.882
315.08	3.023
316.62	3.119
318.16	3.170
319.71	3.198
321.29	3.221
322.90	3.244
324.52	3.270
326.16	3.298
327.80	3.330
329.44	3.358
331.08	3.384
332.72	3.403
334.34	3.416
335.97	3.422
337.60	3.419

Table 2 (*Continued*)

T/K	$\frac{C_p}{J\,K^{-1}g^{-1}}$
339.23	3.407
340.87	3.387
342.52	3.351
344.19	3.298
345.88	3.222
347.62	3.114
349.42	2.979
351.27	2.831
353.19	2.693
355.15	2.580
357.16	2.507
359.18	2.462
361.22	2.439
363.24	2.428
365.25	2.423
367.26	2.424
369.25	2.428
371.25	2.433
373.24	2.439
375.23	2.445
377.22	2.452
379.21	2.454
381.20	2.452
383.20	2.460
385.21	2.464
387.21	2.467
389.21	2.472
Series 2	
85.31	0.605
87.75	0.621
90.39	0.637
93.25	0.654
96.11	0.670
98.97	0.686
101.83	0.706
104.71	0.720
107.59	0.734
110.48	0.751
113.44	0.683
Series 3	
115.78	0.777
117.70	0.788
120.13	0.801
123.05	0.817
125.97	0.833
128.89	0.848
131.81	0.863
134.73	0.878
137.66	0.893
140.58	0.910
143.50	0.925
146.42	0.940
149.35	0.955

Table 2 (*Continued*)

T/K	$\frac{C_p}{J\,K^{-1}g^{-1}}$
152.28	0.971
155.21	0.987
158.14	1.002
161.07	1.020
163.99	1.036
166.91	1.052
169.83	1.069
172.76	1.087
175.68	1.104
178.60	1.122
181.52	1.139
184.44	1.159
187.36	1.176
190.29	1.195
193.21	1.213
196.13	1.232
199.04	1.252
201.95	1.274
204.87	1.294
207.76	1.329
210.65	1.370
213.50	1.411
216.29	1.459
219.02	1.517
221.69	1.586
224.30	1.653
226.85	1.709
229.36	1.762
231.84	1.805
234.27	1.850
236.68	1.890
239.06	1.927
241.41	1.964
243.73	2.000
246.03	2.034
248.32	2.067
250.57	2.100
252.81	2.132
255.03	2.156
257.23	2.186
259.41	2.216
261.58	2.247
263.72	2.278
265.85	2.307
267.95	2.338
270.04	2.369
272.11	2.397
274.16	2.427
276.20	2.459
278.22	2.490
280.22	2.519
282.21	2.550
284.19	2.575

Table 2 (*Continued*)

T/K	$\frac{C_p}{J\,K^{-1}g^{-1}}$
286.14	2.610
288.08	2.640
290.01	2.669
291.92	2.699
293.82	2.726
295.70	2.754
297.58	2.783
299.44	2.808
301.29	2.832
303.14	2.860
304.97	2.884
306.80	2.910
308.61	2.936
310.42	2.963
312.22	2.990
314.00	3.019
315.78	3.048
317.55	3.080
319.30	3.114
321.04	3.149
322.77	3.182
324.48	3.217
326.19	3.246
327.89	3.271
329.59	3.290
331.28	3.302
332.98	3.309
334.68	3.311
336.38	3.312
338.09	3.311
339.80	3.304
341.51	3.284
343.24	3.246
344.98	3.186
346.74	3.098
348.55	2.982
350.40	2.842
352.30	2.687
354.26	2.545
356.28	2.449
358.32	2.408
360.37	2.398
362.43	2.398
364.48	2.401
366.53	2.407
368.58	2.415
370.62	2.422
372.65	2.430
374.69	2.438
376.72	2.444
378.74	2.448
380.77	2.452
382.79	2.454

Table 2 (*Continued*)

T/K	$\frac{C_p}{J\,K^{-1}g^{-1}}$
384.81	2.458
Series 4	
6.61	0.009
7.26	0.012
8.59	0.017
10.45	0.027
12.16	0.036
14.07	0.049
16.17	0.063
18.37	0.079
20.67	0.097
23.06	0.117
25.53	0.137
28.09	0.154
30.54	0.171
Series 5	
7.14	0.011
8.28	0.016
9.73	0.023
11.49	0.032
13.19	0.044
14.94	0.054
16.80	0.068
18.71	0.083
20.66	0.099
22.66	0.115
24.70	0.134
26.78	0.152
28.94	0.168
Series 6	
9.43	0.023
13.23	0.042
15.61	0.057
17.61	0.073
19.72	0.091
21.91	0.108
24.07	0.128
26.22	0.147
28.45	0.164
30.75	0.184
33.06	0.209
35.35	0.228
37.72	0.247
40.15	0.268
42.60	0.289
45.08	0.311
47.58	0.332
50.12	0.353
52.96	0.375
55.29	0.396
57.92	0.417
60.58	0.436
63.26	0.456

Table 2 (*Continued*)

T/K	$\frac{C_p}{J\,K^{-1}g^{-1}}$
65.96	0.476
68.69	0.495
71.43	0.514
74.19	0.532
76.96	0.551
79.75	0.568
82.55	0.586
85.36	0.603
88.18	0.620
91.01	0.637
93.85	0.653
96.71	0.669
99.57	0.685
Series 7	
98.10	0.690
98.20	0.675
99.75	0.689
102.69	0.709
105.57	0.724
108.45	0.737
111.34	0.755
114.23	0.771
117.13	0.787
120.03	0.802
122.94	0.818
125.85	0.833
128.75	0.848
131.66	0.863
134.58	0.879
137.50	0.894
140.41	0.910
143.33	0.926
146.25	0.942
149.17	0.957
152.09	0.973
155.01	0.989
157.93	1.004
160.85	1.022
163.77	1.037
166.69	1.053
169.61	1.070
172.52	1.085
175.39	1.112
178.26	1.099
181.10	1.140
183.88	1.155
186.64	1.176
189.37	1.198
192.07	1.221
194.75	1.242
197.40	1.264
200.03	1.286
202.63	1.307

Table 2 (*Continued*)

T/K	$\frac{C_p}{J\,K^{-1}g^{-1}}$
205.20	1.328
207.75	1.351
210.27	1.375
212.76	1.406
215.21	1.444
217.62	1.490
219.99	1.542
222.31	1.599
224.58	1.656
226.81	1.709
229.00	1.758
231.17	1.801
233.30	1.839
235.42	1.875
237.51	1.908
239.57	1.939
241.62	1.968
243.65	1.994
245.66	2.021
247.66	2.048
249.63	2.077
251.59	2.103
253.54	2.128
255.47	2.150
257.39	2.175
259.29	2.202
261.19	2.228
263.07	2.255
264.94	2.282
266.79	2.309
268.63	2.336
270.45	2.364
272.26	2.390
274.06	2.417
275.84	2.445
277.61	2.472
279.37	2.499
Series 8	
280.24	2.437
280.95	2.497
282.26	2.551
284.16	2.713
286.01	2.803
287.88	2.809
289.78	2.795
291.71	2.793
293.65	2.803
295.59	2.819
297.53	2.840
299.48	2.860
301.44	2.881
303.39	2.902
305.35	2.924

Table 2 (*Continued*)

T/K	$\frac{C_p}{J\,K^{-1}\,g^{-1}}$
307.31	2.946
309.27	2.971
311.24	2.995
313.20	3.023
315.16	3.054
317.13	3.087
319.09	3.124
321.06	3.163
323.02	3.200
324.99	3.236
326.97	3.262
328.95	3.281
330.94	3.282
332.92	3.275
334.91	3.265
336.91	3.253
338.91	3.241
340.91	3.221
342.93	3.185
344.96	3.119
347.03	3.017
349.15	2.883
351.30	2.727
353.47	2.576
355.62	2.462
357.73	2.410
359.79	2.395
361.81	2.395
363.81	2.403
365.80	2.408
367.79	2.412
369.78	2.417
371.77	2.424
373.76	2.432
375.76	2.438
377.75	2.442
379.75	2.446
381.75	2.448
383.75	2.449
385.75	2.456
387.75	2.466
389.74	2.470
391.74	2.477
393.74	2.485
395.74	2.491
397.75	2.496
399.75	2.506
401.75	2.512
403.76	2.518
405.77	2.524
373.76	2.432
375.76	2.438

8 (up to about 300 K) are also affected by relaxation because there was a waiting time of several hours under adiabatic conditions (almost constant temperature) between the end of series 7 and the start of series 8: first a lower heat capacity was observed than the heat capacities measured during series 3 and then the heat capacities were higher.

The results obtained in the temperature range from 350 to 406 K are plotted in Fig. 3. This temperature range represents the end of the melting process and the liquid state. Above 362 K the sample appears to be molten (series 3 and 8). During series 1, however, the end of melting was observed at a slightly higher temperature: 368 K. Above 368 K the results of the series 1, 3 and 8 are in almost perfect agreement with each other, although possibly in the temperature range 368–385 K the heat capacities measured during series 1 are slightly higher than those measured during series 3 and 8. Above approximately 380 K, within experimental error, the measurements are in very good agreement with (estimated) specific heat capacity data of (metastable) liquid LPE as given by Wunderlich and Czornyj [10] (and adopted by Mathot [11]):

$$\frac{c_p(\mathrm{LPE,liq},T)}{\mathrm{J\,K^{-1}\,mol^{-1}}} = 1.426 + 2.401\times10^{-3}\left(\frac{T}{\mathrm{K}}\right) + 7.065\times10^{-7}\left(\frac{T}{\mathrm{K}}\right)^2 \quad (1)$$

Measurements on VLDPE showed a remarkable progressive increase of the specific heat capacity of the polymer in its liquid state between subsequent series of measurements [2]. This phenomenon was not observed for a homogeneous ethylene-1-octene copolymer [3] and for this EB 5 sample.

At the lowest temperatures, see Fig. 4a–b, the specific heat capacities are found to lie in between those for the reference states for completely amorphous and completely crystalline polyethylenes, as expected for a semi-crystalline polyethylene [11,12].

EB 5 shows a clear-cut glass transition, centred around 224 K, which value marks the point of inflection of the heat capacity heating curve. The glass transition of ethylene-based copolymers is known to depend on the type and amount of comonomer [5] and the transition range for EB 5 is situated at lower temperatures as reported for BPE [13]. As typical for the present amount of comonomer, melting starts immediately on devitrification during heating.

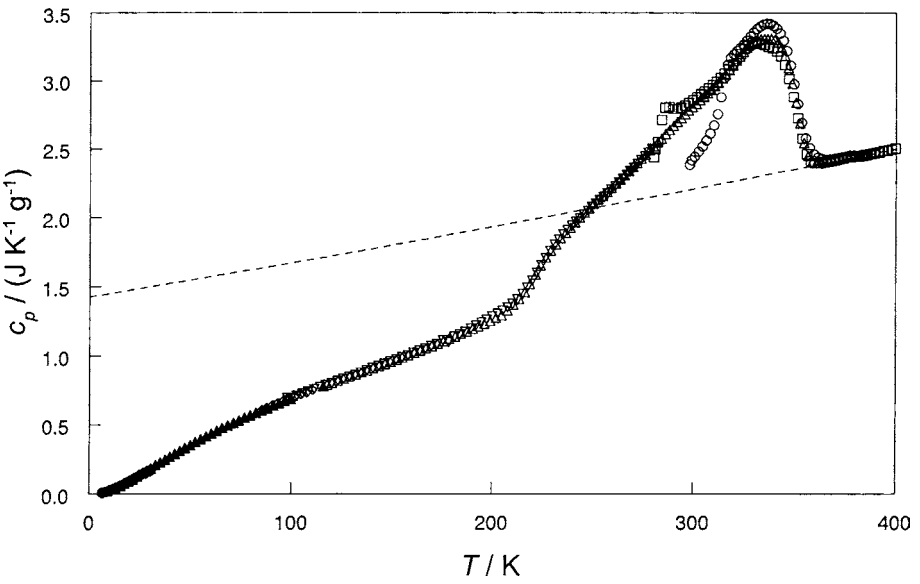

Fig. 2. Specific heat capacity of EB 5 as a function of temperature. Series 1 (sample as received) (○); series 2 (◇); series 3 (△); series 4 (●); series 5 (◆); series 6 (▲); series 7 (▽); series 8 (□). Dashed line, specific heat capacity of (metastable) liquid linear polyethylene (LPE) according to Eq. (1).

3.2. Crystallinity

The enthalpy-based mass fraction crystallinity of EB 5, as defined within the two-phase model, may be calculated using the following equation [12]:

$$w^{c}(T) = \frac{h_a(T) - h(T)}{h_a(T) - h_c(T)} \quad (2)$$

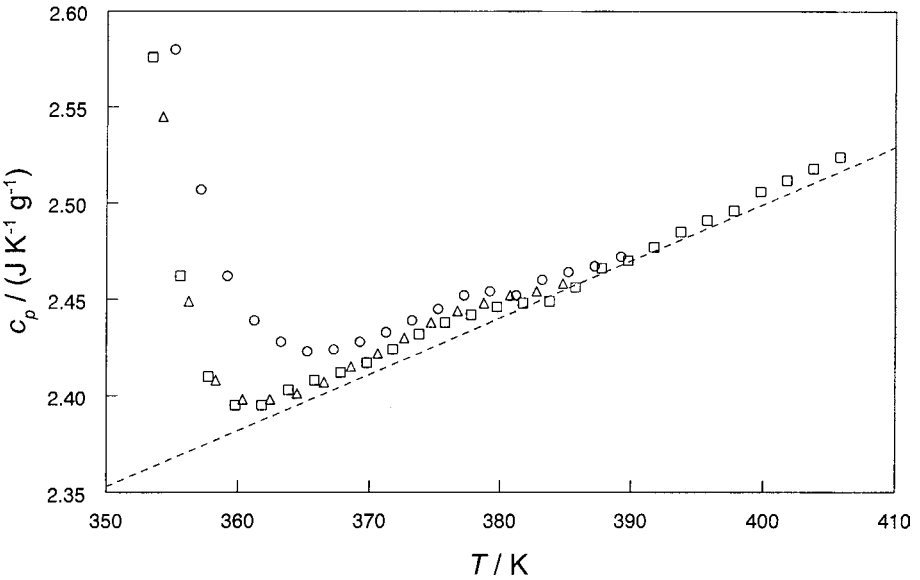

Fig. 3. Specific heat capacity of EB 5 in the liquid state. Series 1 (sample as received) (○); series 3 (△); series 8 (□). Dashed line, specific heat capacity of (metastable) liquid linear polyethylene (LPE) according to Eq. (1).

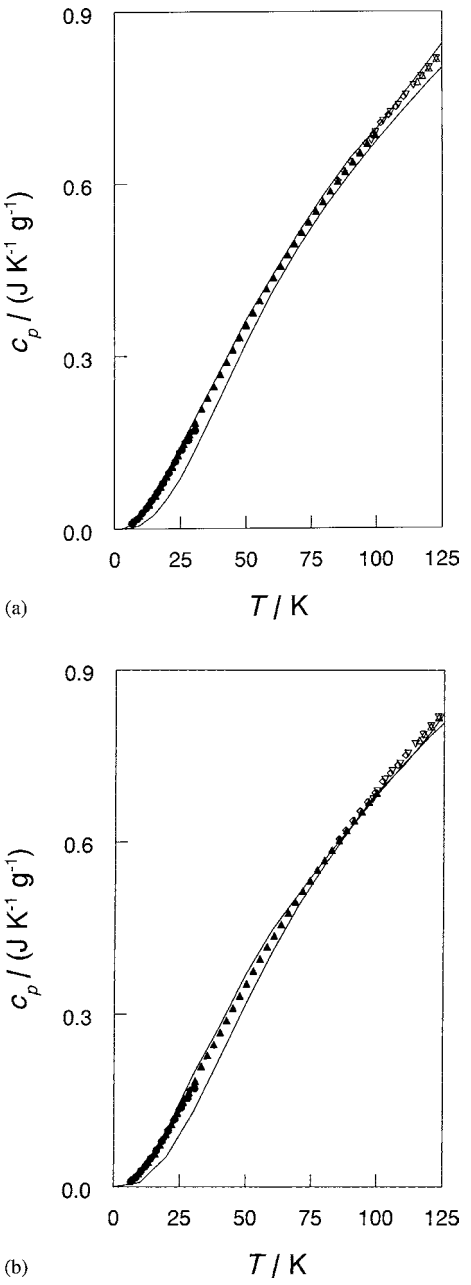

Fig. 4. Low temperature specific heat capacity data for EB 5. Series 2 (◇); series 3 (△); series 4 (●); series 5 (◆); series 6 (▲); series 7 (▽). (a) The solid lines represent specific heat capacity data for completely crystalline and completely amorphous polyethylene (BPE) according to the ATHAS data bank [13]; (b) the solid lines represent the data for completely amorphous and completely crystalline LPE according to Mathot [11]. Specific heat capacities for the completely amorphous phase are higher than those for the completely crystalline phase.

In this equation, $h_a(T)$ is the specific enthalpy of the completely amorphous phase, $h_c(T)$ the specific enthalpy of the completely crystalline phase and $h(T)$ the specific enthalpy of the semi-crystalline sample. Because the enthalpy function does not have a natural zero-point (see e.g. [14]) a common reference point has to be defined. Here, the specific enthalpy of EB 5 at a temperature of 400 K is selected as the reference point for the enthalpy function. At $T = 400$ K EB 5 is completely molten; therefore, it may be stated that $h_a(T = 400\,\mathrm{K}) = h(T = 400\,\mathrm{K})$.

The specific enthalpy as a function of temperature is found by integrating the specific heat capacity:

$$h(T = \Theta) - h(T = 400\,\mathrm{K}) = \int_{T=400\,\mathrm{K}}^{T=\Theta} c_p(T)\,\mathrm{d}T \quad (3)$$

It is assumed here that the specific enthalpy of the crystalline phase is equal to the specific enthalpy of completely crystalline LPE as given by Mathot [11], corrected for the difference in reference point. The specific enthalpy of the amorphous phase is calculated using Eq. (3) by assuming that:

- the glass transition temperature is $T_g = 224$ K;
- the specific heat capacity of the amorphous phase above the glass transition temperature is equal to the specific heat capacity of (super-cooled) liquid LPE (given by Eq. (1));
- the specific heat capacity of the amorphous phase below the glass transition temperature is equal to the specific heat capacity of amorphous BPE in its glassy state as given by the ATHAS data bank [13].

The heat capacities used to evaluate the specific enthalpies are plotted in Fig. 5. The Fig. 6 represents a plot of the specific enthalpies thus found together with the enthalpy-based mass fraction crystallinity calculated using Eq. (2). In the temperature range from 220 to 360 K the crystallinity gradually decreases from 0.30 to zero, caused by melting of the crystalline phase. Vanden Eynde [4] calculated the crystallinity of EB 5 from DSC heating curves (after cooling at 10 K min^{-1}): she found crystallinities of 0.26 at 233 K, 0.22 at 273 K and 0.17 at 293 K whereas our values at the same temperatures are slightly higher: 0.28, 0.24 and 0.19, respectively. This small difference is probably caused by the much smaller cooling rates in our experiments.

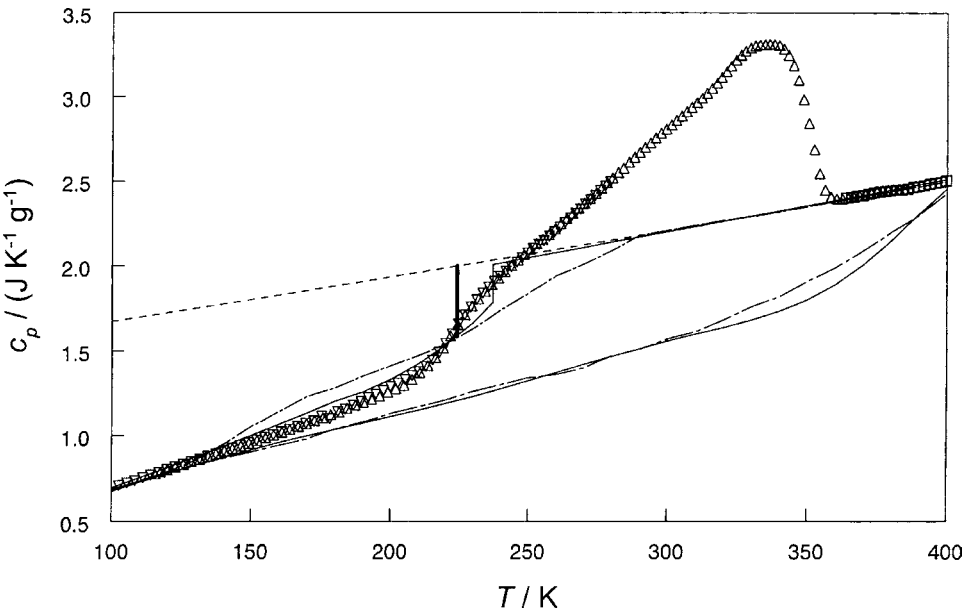

Fig. 5. Specific heat capacity data for EB 5 in the glass transition and melting region. Series 3 (△); series 7 (▽); series 8 (□). The solid and the dash-dotted lines represent reference data for BPE according to the ATHAS data bank [13] and for LPE according to Mathot [11], respectively. Reference data are given for completely amorphous and for completely crystalline phases. The dashed line represents the specific heat capacity of (metastable) liquid LPE according to Eq. (1). The thick vertical line at $T = 224$ K represents the assumed heat capacity step for completely amorphous material at the glass transition temperature (see text).

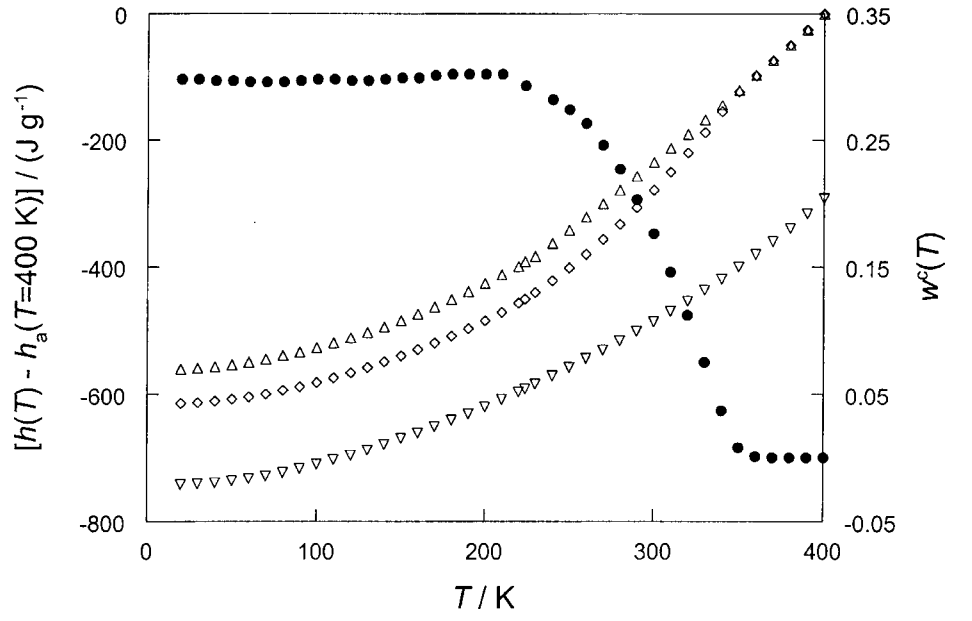

Fig. 6. Specific enthalpy of the semi-crystalline EB 5 sample (◇), together with the specific enthalpy of the crystalline phase (▽) and of the amorphous phase (△). The enthalpy-based mass fraction crystallinity (scaling given on the right vertical axis) of the EB 5 sample is also plotted (●).

3.3. Base line and excess heat capacities

The so-called specific base-line heat capacity (c_{pb}) [12] of EB 5 may be calculated using the evaluated crystallinity as a function of temperature and the following equation:

$$c_{pb}(T) = w^{c}(T)c_{pc}(T) + [1 - w^{c}(T)]c_{pa}(T)$$

where c_{pc} and c_{pa} are the specific heat capacities of the completely crystalline and completely amorphous phases, respectively. Successively, the specific excess heat capacity (c_{pe}) [12] can be calculated by subtracting the specific base-line heat capacity from the experimental specific heat capacity:

$$c_{pe}(T) = c_{p}(T) - c_{pb}(T)$$

A plot of the specific base-line heat capacity and the specific excess heat capacity of EB 5 as a function of temperature is presented in Fig. 7.

3.4. Temperature drifts during stabilisation periods in the melting region

Temperature drifts of the sample and calorimeter vessel in the melting region were evaluated from linear fits of the temperature versus time curves in the second half of the stabilisation periods. The temperature drifts of measurement series 1, 3, 7, and 8 are plotted in Fig. 8. In a transition region characterised by an endothermic heat effect, such as melting, negative drifts are usually observed. The negative drifts for series 1 (up to $-180\ \mu K\ s^{-1}$) and series 8 with local minima at approximately 315 and 285 K, respectively, are related to the temperatures at which annealing took place (room temperature and 280 K, respectively) and to the time it took (some years for series 1 and some hours for series 8). During series 1, 3, and 8, however, at higher temperatures (above approximately 340 K for series 1 and above approximately 325 K for series 3 and 8) also positive temperature drifts were detected (see Fig. 8). This implies that in this part of the melting region a relaxation process occurs in the stabilisation periods, which must be intermitted as recrystallisation.

These observations for EB 5 are in agreement with the results that were obtained for a homogeneous ethylene-1-octene copolymer (EOM) [3] as well as for a heterogeneous ethylene-1-octene very low-density polyethylene [2].

Obviously, the longer the time spent in annealing, and/or the slower the cooling rate before subsequent melting, the more stable the material will be for an increasing temperature range above the annealing temperature. In these cases, during heating, possibilities of recrystallisation are decreased or even prohibited; in the latter case only melting is left.

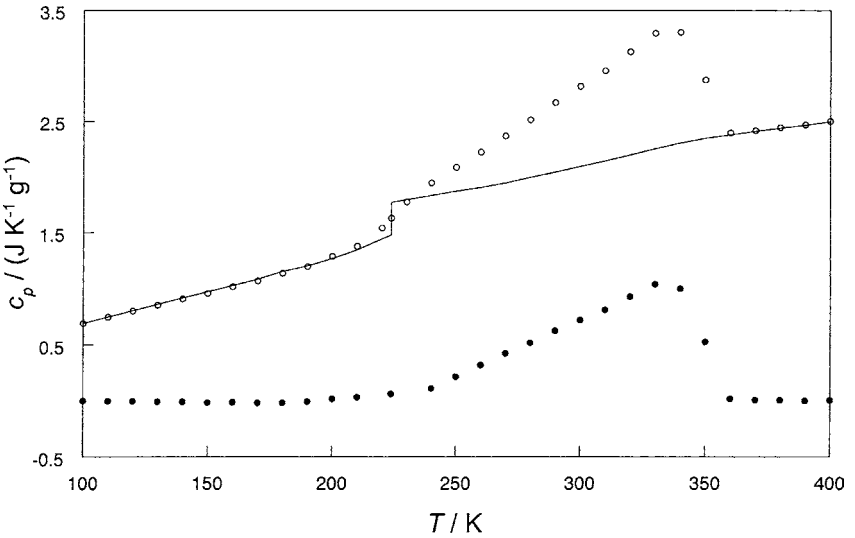

Fig. 7. Experimental specific heat capacity of EB 5 (○) together with the specific base-line heat capacity (solid line) and the specific excess heat capacity (●).

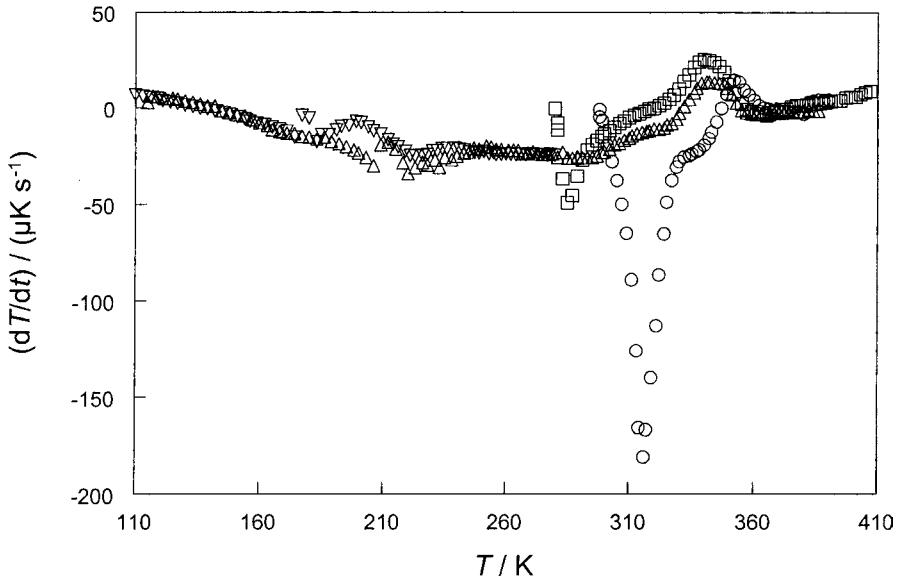

Fig. 8. Temperature drifts observed during the stabilisation periods. Series 1 (○) (sample as received); series 2 (△); series 3 (◇); series 8 (□).

As stated in our paper presenting the results of measurements on a homogeneous ethylene-1-octene copolymer [3], the observed phenomena link up with temperature-modulated differential scanning calorimetry (TMDSC) experiments in which, depending on the thermal history, also excess phenomena are seen [15–17].

References

[1] V.B.F. Mathot (Ed.), Calorimetry and Thermal Analysis of Polymers, Cart Hanser, Munich, 1994.
[2] J.C. van Miltenburg, V.B.F. Mathot, P.J. van Ekeren, L.D. Ionescu, J. Therm. Anal. Cal. 56 (1999) 1017.
[3] P.J. van Ekeren, L.D. Ionescu, V.B.F. Mathot, J.C. van Miltenburg, J. Therm. Anal. Cal. 59 (2000) 683.
[4] S. Vanden Eynde, Homogeneous Ethylene-1-Alkene Copolymers: A Study of the Crystallisation and Melting Behaviour at Ambient and Elevated Pressures, Thesis Katholieke Universiteit Leuven, 1999.
[5] S. Vanden Eynde, V. Mathot, M.H.J. Koch, H. Reynaers, Polymer 42 (2000) 3437.
[6] J.C. van Miltenburg, G.J.K. van den Berg, M.J. van Bommel, J. Chem. Thermodyn. 19 (1987) 1129.
[7] J.C. van Miltenburg, A.C.G. van Genderen, G.J.K. van den Berg, Thermochim. Acta 319 (1998) 151.
[8] H. Preston-Thomas, Metrologia 27 (1990) 3.
[9] R.N. Goldberg, R.D. Weir, Pure Appl. Chem. 64 (1992) 1545.
[10] B. Wunderlich, G. Czornyj, Macromolecules 10 (1977) 906.
[11] V.B.F. Mathot, Polymer 25 (1984) 579.
[12] V.B. F. Mathot, Thermal Characterisation of States of Matter, in: V.B.F. Mathot (Ed.), Calorimetry and Thermal Analysis of Polymers, Cart Hanser, Munich, 1994, p. 105 (Chapter 5).
[13] ATHAS data bank, B. Wundelich, Pure Appl. Chem. 67 (1995) 1019. Detailed information may also be found on the internet: http://web.utk.edu/∼athas.
[14] P.J. van Ekeren, Thermodynamic background to thermal analysis and calorimetry, in: M.E. Brown (Ed.), Handbook of Thermal Analysis and Calorimetry: Principles and Practice, Vol. 1, Elsevier, Amsterdam, 1998, p. 75 (Chapter 2).
[15] R. Scherrenberg, V. Mathot, A. van Hemelrijck, Thermochim. Acta 330 (1999) 3.
[16] R. Androsch, Polymer 40 (1999) 2805.
[17] A. Wurm, M. Merzlyakov, C. Schick, Thermochim. Acta 330 (1999) 121.